applied sciences

MDPI

Article

Separation of Zr from Zr-2.5Nb by Electrorefining in LiCl-KCl for Volumetric Decontamination of CANDU Pressure Tube

Jungho Hur [1], Seongjin Jeong [2], Sungjune Sohn [3,*], Jaeyeong Park [1] and Il Soon Hwang [2]

[1] School of Mechanical, Aerospace and Nuclear Engineering, Ulsan National Institute of Science and Technology, Ulsan 44919, Korea; junghohur@unist.ac.kr (J.H.); jypark@unist.ac.kr (J.P.)

[2] Department of Energy System Engineering, Seoul National University, Seoul 08826, Korea; dydqusduvh@snu.ac.kr (S.J.); hisline@snu.ac.kr (I.S.H.)

[3] Decommissioning Technology Research Division, Korea Atomic Energy Research Institute, Daejeon 34057, Korea

* Correspondence: sjsohn@kaeri.re.kr; Tel.: +82-42-868-4780

Abstract: This study presents an experimental investigation on Zr separation from Zr-2.5Nb by anode potentiostatic electrorefining in LiCl-KCl-$ZrCl_4$ 0.5 wt. % at 773 K for irradiated CANDU pressure tube decontamination. By the ORIGEN-2 code calculation, radioactive characteristics were investigated to show that Nb-94 was the most significant radionuclide with an aspect of waste level reduction by electrorefining. Three electrorefining tests were performed by fixing the applied potential as −0.9 V (vs. Ag/AgCl 1 wt. %) at the anode to dissolve only Zr. A cathode basket was installed to collect detached deposits from the cathode. Electrorefining results showed Zr was deposited on the cathode with a small amount of Nb and other alloying elements. The chemical form of the cathode deposits was shown to be only Zr metal or a mixture of Zr metal and ZrCl, depending on the experimental conditions related to the surface area ratio of the cathode to the anode. It was determined that the Zr metal reduction at the cathode was attributed to the two-step reduction reaction of Zr^{4+}/ZrCl and ZrCl/Zr.

Keywords: Zr recovery; CANDU pressure tube; Zr-2.5Nb; electrorefining; molten salt; LiCl-KCl; nuclear power plant decommissioning; radioactive waste

check for updates

Citation: Hur, J.; Jeong, S.; Sohn, S.; Park, J.; Hwang, I.S. Separation of Zr from Zr-2.5Nb by Electrorefining in LiCl-KCl for Volumetric Decontamination of CANDU Pressure Tube. *Appl. Sci.* **2021**, *11*, 3790. https://doi.org/10.3390/app11093790

Academic Editor: Bruno Merk

Received: 13 March 2021
Accepted: 20 April 2021
Published: 22 April 2021

1. Introduction

Zr alloy has been extensively used in nuclear fuel cladding, since Zr has corrosion resistance and a low neutron capture cross-section [1,2]. The CANDU pressure tube is made of Zr-2.5Nb alloy to endure high temperature, pressure, and radioactivity during its long-term operation. However, Nb-93, the most stable niobium, can be activated into Nb-94, which emits beta radiation with a long half-life of 20,300 years under high neutron flux. In the Republic of Korea (ROK), Nb-94 is one of the most crucial isotopes in the geological disposal of irradiated Zr-Nb alloy. The activity concentration limit of Nb-94 for the Gyeongju low- and intermediate-level waste (LILW) disposal facility is much smaller than the radioactivity caused by Nb-94 in several types of irradiated Zr-Nb components [3,4]. Moreover, Wolsong unit 1, a CANDU-6-type nuclear power plant (NPP) in the ROK, was permanently shut down from 2019. Hence, the irradiated CANDU pressure tube, which can be classified as intermediate-level waste (ILW), should be decontaminated by separating Zr from the alloy to reduce the final radioactive waste volume as well as its waste level.

Since Nb-94 is uniformly distributed in the irradiated pressure tube volume, volumetric decontamination is required to separate Zr from Zr-Nb alloy, leaving behind Nb. Rudisill et al. performed the surface treatment on irradiated Zircaloy cladding by using HF, but it was revealed that the surface decontamination could not eliminate the actinides and fission products that deeply penetrated the cladding [5]. Halogenation methods have been investigated on Zr alloys in the nuclear energy industry since Zr refinement was commercially developed [6–10]. In terms of Zr-2.5Nb alloy, however, they can accompany secondary radioactive waste generation, such as chloride gas related to C-14. Besides, corrosion issues may occur in industrial-scale reactor structural materials due to Cl_2 and HCl.

For this reason, electrorefining using molten halide electrolytes has been studied for the volumetric treatment of metallic radioactive waste [11–19]. Previous electrorefining tests in fluorides have shown that it is possible to recover metallic Zr deposits as a dendrite from on the cathode with high purity due to the single-step Zr reduction reaction in fluorides [11–13]. Park et al. conducted the electrorefining of Zirlo, containing Nb of 1 wt. % in Zr alloy, in molten LiF-KF-ZrF_4 salt at 973 K, and they achieved an Nb concentration in the cathode deposit of less than 30 ppm [11]. Fujita et al. conducted the electrorefining of a BWR channel box in molten LiCl-KCl-$ZrCl_4$-ZrF salt at 923 K to separate Co-60 [12]. Lee et al. conducted the electrorefining of Zirlo in fluoride-added chloride salt to recover pure Zr, with a coarse deposit formed at the cathode [13]. Despite this advantage, fluorides have high corrosivity to structural materials, and it is required that a high operating temperature is used due to its melting point, which can potentially lead to scale-up issues. In terms of the chloride process, it has been reported that Zr shows multiple redox steps in chlorides which can affect process throughput [14–17]. However, experimental and computational studies on Zircaloy-4 electrorefining showed that a high separation efficiency for Zr can be achieved by potentiostatic methods [18–20]. In addition, chlorides have less corrosivity and lower melting points than fluorides.

Herein, in this study, we performed the Zr separation from Zr-2.5Nb alloy by electrorefining in molten LiCl-KCl-$ZrCl_4$ salt with a variation in cell design in terms of cathode surface area and presence of the cathode basket. Three electrorefining tests were carried out to investigate the change in the cathode. The chemical form of the cathode deposit mixture was identified by X-ray diffractometry (XRD). Quantitative analysis on the cathode deposits obtained from the two tests was performed by inductively coupled plasma-mass spectrometry (ICP-MS).

2. Radioactive Characteristics of Irradiated CANDU Pressure Tube

By using the ORIGEN-2 code, activation simulation was performed for the CANDU pressure tube. ORIGEN-2 could calculate the radioactivity, concentration, and decay heat of activation products in the irradiated CANDU pressure tube [21]. It was assumed that the pressure tube was irradiated by neutron activation for 30 years, based upon actual CANDU operating experience [22]. The neutron flux was set to 1×10^{14} n/(cm^2 s). The composition of nuclear grade Zr-2.5Nb was referred to from the ASTM B353-12 [23].

Figure 1 shows the ratio of radioactivity in the irradiated CANDU pressure tube to the activity concentration limit for LLW disposal in the ROK with cooling time. The ratio higher than 1 means the activity of radionuclides exceeded the LLW criteria. It was revealed that three radionuclides, Nb-94, C-14, and Co-60, had higher radioactivity than the limit. Co-60 is produced by the neutron activation of Co-59 and rapidly undergoes radioactive beta decay with a short half-life of 5.27 years. For this reason, the radioactivity of Co-60 in the discharged pressure tube can decrease below the concentration limit after a cooling period of 10 years. Based on the NPP decommissioning plan in the ROK, decommissioning will begin after 10 years from the reactor shutdown, planning, and administrative period. Therefore, Co-60 is not a significant radionuclide in terms of pressure tube decontamination.

C-14 is mainly generated by the neutron activation of N-14 and decays with a long half-life of 5730 years. Nb-94, generated by the neutron activation of Nb-93, has the longest half-life, of 20,300 years, among the major radionuclides. After 10 years from the discharge, it was shown that C-14 and Nb-94 had 4.4 and 7.5×10^4 times higher radioactivity than the limits, respectively. In addition, the half-life values of C-14 and Nb-94 are so long that the radioactivity cannot rapidly decrease as depicted in Figure 1. Considering that metal structural wastes generated from the NPP decommissioning require long-term disposal in the underground facility, C-14 and Nb-94 are regarded as the most important isotopes for the management of the irradiated CANDU pressure tube.

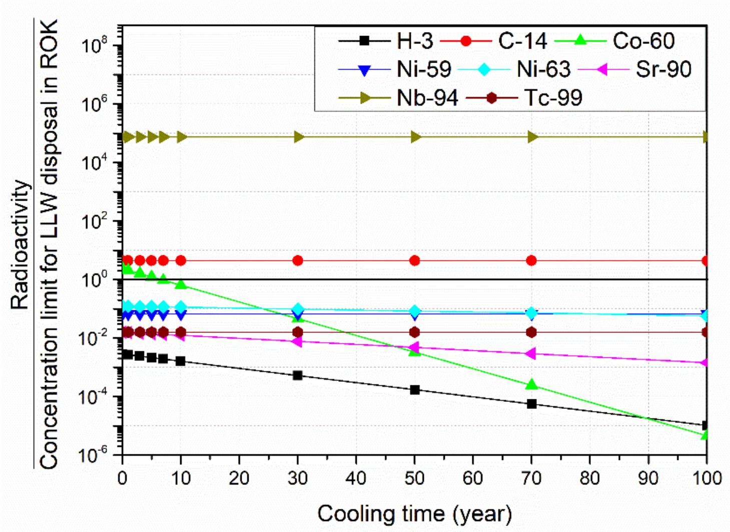

Figure 1. The ratio of radioactivity in the irradiated CANDU pressure tube after operating for 30 years to activity concentration limit for LLW disposal in ROK with cooling time.

During the electrorefining process, it is expected that C-14 is detached as a particle form from the anode material, the CANDU pressure tube, without any ionization. This can enable C-14 to be easily retrieved within the molten salt system. Nb-94 which exists in the metal phase is dissolved from the anode by electrolytic methods. Therefore, we mainly focused on the separation between Zr and Nb in the Zr-2.5Nb alloy by electrorefining.

3. Experimental

3.1. Reagents and Apparatuses

A glove box was filled and continually purged with inert argon gas of 99.999% purity throughout all experiments. Oxygen and moisture concentration was maintained below 1 ppm with continuous monitoring. The furnace made of Type 304 stainless steel was installed by connecting with the glove box floor. Two jacket heaters surrounded the furnace to provide and maintain a stable temperature. The temperature was controlled by using a proportional integral derivative controller. All electrochemical measurements were conducted by utilizing a Versastat3 potentiostat (Princeton Applied Research).

LiCl-KCl eutectic salt (Sigma-Aldrich, 99.99% purity) was used as an electrolyte. $ZrCl_4$ (Sigma-Aldrich, 99.99% purity) was introduced into LiCl-KCl to provide Zr. Total amount of electrolyte was set to be 40 g for each test. Two types of tungsten rod (Sigma-Aldrich, 99.99% purity, 1 mm diameter; Alfa Aesar, 99.95% purity, 3.175 mm diameter) were used for the cathode. An Ag/AgCl 1 wt. % electrode was produced as a reference electrode by immersing Ag wire (Sigma-Aldrich, 99.99% purity, 1 mm diameter) into 1 wt. % AgCl (Sigma-Aldrich, 99.999% purity) in LiCl-KCl contained in a Pyrex tube with a thin tip. A tubular quartz cell, which had an inner diameter of 27 mm and a height of 40 cm, was used for the electrorefiner. Zr-2.5Nb alloy of 3.14 g was used for anode material. An anode basket, made of Type 316 stainless steel, was utilized as a container for chopped Zr-2.5Nb pieces. To prevent the drop of electrodeposited Zr particles, cathode baskets made of alumina or quartz were employed. A thin quartz tube was utilized as an insulator for the anode and cathode rod.

3.2. Methods

The objective of the electrorefining was to recover pure Zr from Zr-2.5Nb alloy without co-deposition of Nb on the cathode. It was reported that Zr and Nb have various ion states in molten LiCl-KCl salt, investigated by cyclic voltammetry [14–17,24–26]. Although this shows complicated redox behaviors, the standard reduction potential of soluble/insoluble reactions are far from each other. Since the standard reduction potential of the reduction reaction into Nb metal is more positive than that of the reduction reaction into Zr metal, the anodic dissolution of Nb can be controlled by applying a specific potential to the anode. On the other hand, once Nb is dissolved into the electrolyte, the electrodeposition of Nb is more dominant than that of Zr at the cathode. If Nb cannot be dissolved from the anode, a high purity of Zr can be electrodeposited on the cathode. For this reason, we determined to perform potentiostatic electrorefining with a fixed potential of -0.9 V (vs. Ag/AgCl 1 wt. %) at the anode to suppress Nb oxidation, that is, to intend only Zr oxidation. Other alloying elements and activation products such as Fe, Ni, and Co were not considered because their compositions were too low to influence Zr [23]. In addition, their standard potentials were significantly far from that of Zr [16].

A previous study showed that Zr deposited on the cathode can be easily detached and settled to the bottom [19]. Additionally, it is possible that Nb can be dropped out of the anode when Zr is being dissolved into molten salt for a long time, until most of the Zr is depleted during anode potentiostatic electrorefining. This indicates that residual anode materials and recovered cathode products could be co-precipitated at the bottom of the electrorefiner. Therefore, a basket was installed for surrounding the cathode in an electrorefining cell to separate possible precipitates from the anode and cathode, as shown in Figure 2. As a reference case, electrorefining test 1 was performed with only an anode basket, containing chopped Zr-2.5Nb alloy. The diameter of the cathode tungsten was 1 mm. Then, a cathode basket was installed for electrorefining tests 2 and 3 to collect precipitate at the bottom. Two different tungsten rods with diameters of 1 and 3.175 mm were employed in tests 2 and 3, respectively, to find out the change in the chemical form of deposited Zr. All electrorefining was conducted in the electrolyte of LiCl-KCl-$ZrCl_4$ (0.5 wt. %). The temperature was fixed at 773 K.

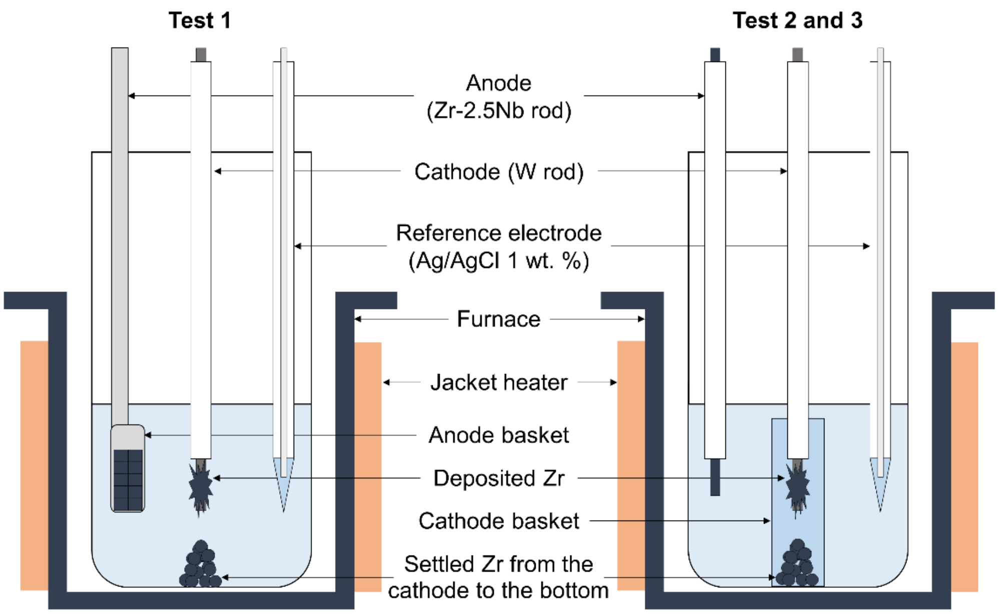

Figure 2. Schematic diagram of electrorefining cell utilized in tests 1–3.

4. Results

In electrorefining tests 1 and 2, a sufficient amount of cathode deposit could not be recovered. The amount was too little to use for XRD analysis. Instead, black powdery precipitate was found at the bottom of the electrorefining cell and cathode basket in tests 1 and 2, respectively, as shown in Figures 3a and 4a. By XRD analysis, Zr metal and ZrO_2 phase were identified in both precipitates, as shown in Figures 3b and 4b.

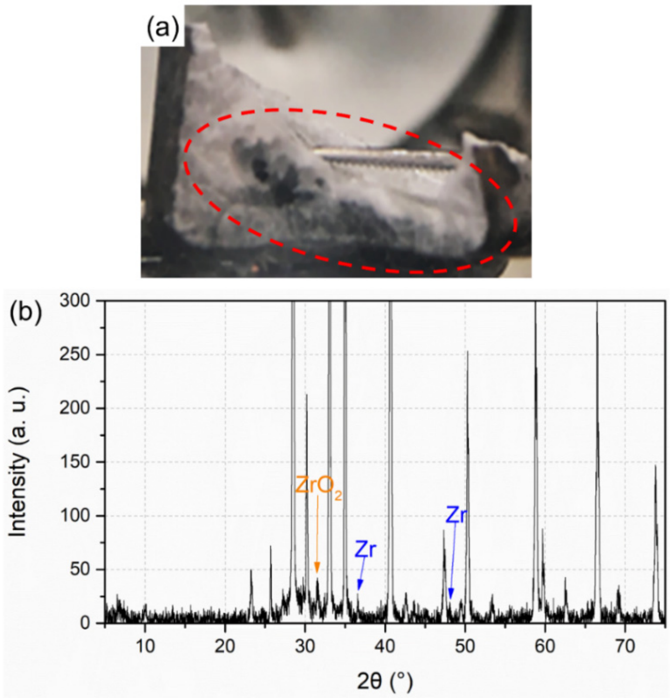

Figure 3. (**a**) Salt ingot obtained from the electrorefining cell in test 1; (**b**) XRD pattern of the black precipitate at the bottom of the salt ingot, represented as a red circle in Figure 3a.

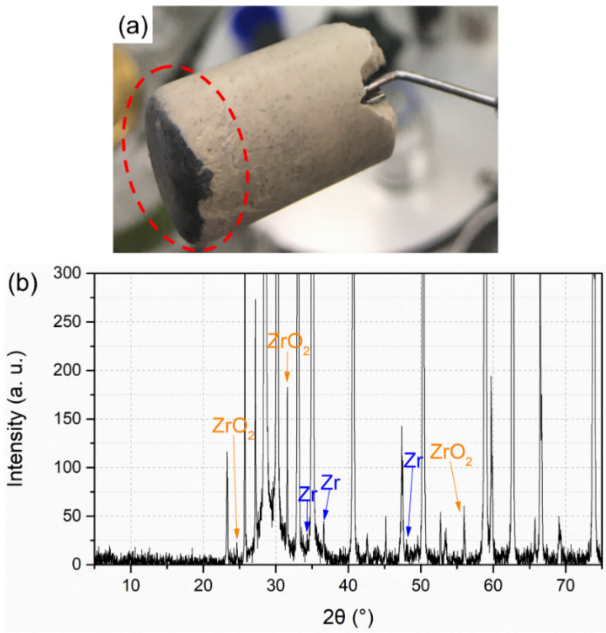

Figure 4. (**a**) Salt ingot obtained from the cathode basket in test 2; (**b**) XRD pattern of the black precipitate at the bottom of the salt ingot, represented as a red circle in Figure 4a.

Unlike tests 1 and 2, plenty of cathode deposits could be recovered in electrorefining test 3 as shown in Figure 5a. Additionally, the precipitate was collected at the bottom of the salt ingot obtained from the cathode basket, as shown in Figure 5b. The cathode deposit was analyzed to be a mixture of ZrCl, Zr, and ZrO_2 by XRD, as shown in Figure 5c.

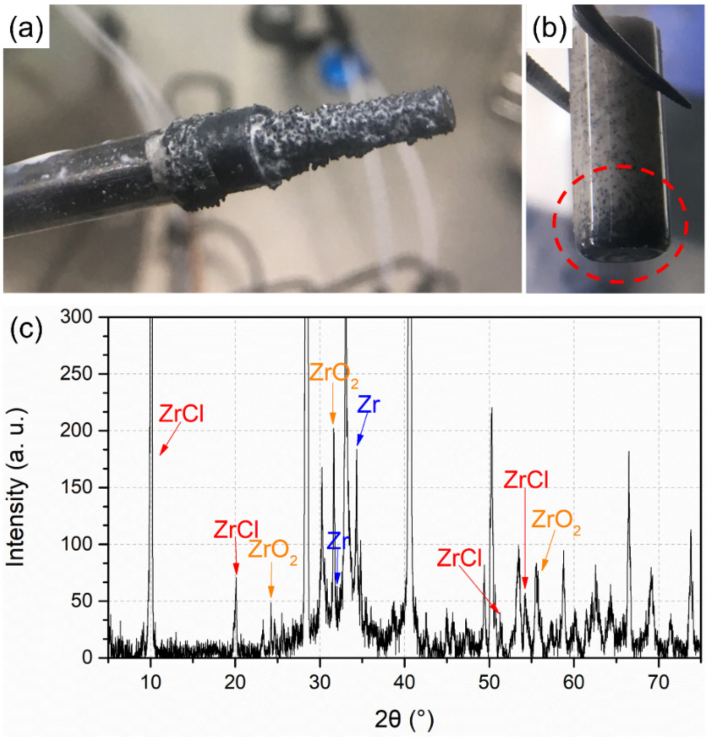

Figure 5. (**a**) Cathode deposit in test 3; (**b**) salt ingot obtained from the cathode basket in test 3; (**c**) XRD pattern of the cathode deposit.

Quantitative measurement was conducted by ICP-MS for the precipitates recovered from tests 1–3. Table 1 represents concentrations of alloying elements in Zr-2.5Nb such as Nb, Fe, Co, and Ni. The concentrations of Nb and Co were shown to be very low in all tests. The concentrations of Fe and Ni were analyzed to be within the range of 10 to 30 ppm.

Table 1. Concentrations of Nb, Fe, Co, and Ni in the precipitates after the tests 1–3.

Origin of Precipitates	Concentration (ppm)			
	Nb	Fe	Co	Ni
Bottom of the cell in test 1	N/D	12.01	N/D	15.55
Bottom of the cathode basket in test 2	0.24	17.36	0.15	23.22
Bottom of the cathode basket in test 3	1.26	27.77	0.03	14.05

5. Discussion

5.1. Chemical Form in Cathode Deposit

ZrO_2 was represented in all XRD patterns, which were obtained from tests 1–3. It was estimated that the ZrO_2 phase was formed by the oxidation of Zr while preparing and conducting XRD analysis in the air atmosphere outside the glove box, because the O_2 concentration was maintained below 1 ppm in the glove box. The precipitate was attributed to the Zr metal detached from the cathode surface in test 1 and 2. In test 3, it was found that ZrCl and Zr were co-deposited on the cathode.

It has been known that Zr has two soluble states, Zr^{4+} and Zr^{2+}, and two insoluble states, ZrCl and Zr, in molten LiCl-KCl salt [14–18]. According to the cyclic voltammogram of $ZrCl_4$ in LiCl-KCl at 773 K, three peaks arise at the cathodic side and the corresponding reactions are represented in order of reduction tendency as follows [15,16]:

$$Zr^{4+} + 2e = Zr^{2+} \tag{1}$$

$$Zr^{4+} + 3e + Cl^{-} = ZrCl \tag{2}$$

$$ZrCl + e = Zr + Cl^- \quad (3)$$

If Zr metal is deposited on the cathode during the electrorefining, that can be explained by two kinds of Zr reduction mechanism under the presence of Zr^{4+} in the chloride electrolyte as follows:

1. Zr^{2+} generation from Zr^{4+} by Equation (1), which is followed by a disproportionate reaction where Zr^{2+} produces Zr^{4+} and Zr metal as shown in Equation (4);

$$2Zr^{2+} = Zr^{4+} + Zr \quad (4)$$

2. ZrCl generation from Zr^{4+} by Equation (2), which is followed by a ZrCl consumption reaction to produce Zr metal by Equation (3).

In the voltammogram, cathodic peaks related to the reduction reactions 2 and 3 were clearly recognized regardless of $ZrCl_4$ concentrations [16]. The cathodic peak related to the reduction Equation (1) (R1) seemed to be distinct in high $ZrCl_4$ concentrations, whereas R1 had a flat shape in low $ZrCl_4$ concentrations. Moreover, as scan rate decreased, R1 could not be distinguished as a peak shape, and the reduction current was very low. This indicated that Zr^{4+} tended to be directly reduced to ZrCl by Equation (2) in a low concentration of $ZrCl_4$ such as 0.5 wt. %, equivalent to the concentration employed in this study. Therefore, in tests 1 and 2, it was estimated that Zr metal was produced not by the first but by the second mechanism associated with Equations (2) and (3). Additionally, in order to cause the Zr metal formation by Equations (3), it was determined that a sufficiently low electrode potential was applied to the cathode. Meanwhile, cell designs utilized in the electrorefining did not include a stirring system and even had a cathode basket. These factors hinder mass transfer and cause large overpotential to the cathode, which could be evidence of the estimation that Equation (3) occurred at the cathode in tests 1 and 2. In addition, the color of molten salt could be another reason that Equation (1) did not occur at the cathode. Based on the literature, it was reported that the molten salt was shown to have a brown color if Equation (1) progressed [14,27]. In tests 1–3, all salt ingots had a white color, as shown in Figures 3–5. Therefore, it is obvious that the Zr metal reductions in tests 1 and 2 could be attributed to Equation (3).

ZrCl and Zr were co-deposited on the cathode in test 3. The surface area of the cathode in test 3 was approximately 3.2 times larger than that in tests 1 and 2. Additionally, tests 2 and 3 utilized a Zr-2.5Nb rod, whereas test 1 utilized chopped Zr-2.5Nb cuts. These experimental preparations enabled test 3 to have the highest surface area ratio of the cathode, as a counter electrode, to the working electrode, as a working electrode, among the three electrorefining tests. For this reason, a relatively small overpotential was driven to the cathode in test 3, rather than tests 1 and 2. As a result, the potential, which allowed both ZrCl and Zr to be electrodeposited, could be applied to the cathode.

5.2. Composition in Cathode Deposit

As represented in Table 1, Nb could be easily suppressed at the Zr-2.5Nb anode; however, Fe and Ni were deposited at the cathode against expectations. This trend was consistent across all tests. Since the standard reduction potential of Nb, Fe, Co, and Ni was −1.61, −1.473, −1.279, and −1.299 V (vs. Cl_2/Cl^-), respectively, the oxidation tendency of Nb was stronger than that of other alloying elements [16,26]. The composition of Nb in the cathode deposit was much higher than that of the others as well. This could cause the difference of anodic equilibrium potential between Nb and alloying elements to become wider. Therefore, if a very small amount of Nb was dissolved from the anode and deposited on the cathode, it was reasonable to consider that Fe, Co, and Ni were not dissolved from the anode at all. The deposited content of Fe and Ni could be regarded as background impurities in the initial LiCl-KCl salt.

The concentrations of Nb were analyzed to be much lower than in the literature [12]. They were involved with a low applied current density on the anode specimen. Hence, the anodic potential could be maintained below the redox potential of Nb during the electrorefining. Unlike a lab-scale experiment, a pilot- or commercial-scale process desires a high current density which results in a high throughput, and that would induce the anode potential rise. An enhanced mass transfer using an electrolyte mixing system, such as rotating electrodes, stirrers, and baffles, can mitigate the potential elevation at the anode. Additional investigations with experimental and computational approaches are required to quantify the stirring effects on the potential change.

5.3. Zr Recovery Yield

All electrorefining tests showed that the Zr deposit was detached from the cathode into the molten salt electrolyte. For this reason, it was difficult to clarify the Zr recovery yield by measuring the mass of the deposit at the cathode directly. If the salt ingot, containing the dropped Zr deposit at the bottom, was dissolved in water, Zr precipitates could be easily filtered. However, the Gibbs free energy of formation and the equilibrium constant for Equation (5) were -565.44 kJ/mol and 1.178×10^{99} at 293 K based on the HSC Chemistry 8.0 calculation. This indicates that Zr metal was highly oxidized in aqueous media. Since the oxidation occurs at the surface of the Zr metal particle, it would be not appropriate to specify that all Zr metal is converted into ZrO_2. Material loss might occur during the dissolution and filtration as well. Therefore, this method is far from a direct filtration of Zr in the inert atmosphere at high temperature, which is much more accurate for estimating Zr recovery yield.

$$Zr + 2H_2O = ZrO_2 + 2H_2 \quad (5)$$

In order to identify the recovery yield indirectly, a passed charge during the electrorefining was utilized to calculate the amount of reducing metal with an assumption that the current efficiency was 100%. The passed charge was 2520 C for 24 h and that was equivalent to 0.5956 g of Zr metal in test 1. In tests 2 and 3, however, 230 and 410 C passed for 24 and 72 h, respectively. These were equivalent to 0.0544 and 0.0969 g. These small charge values were attributed to poor mass transfer during the electrorefining because the cathode basket was a closed structure that did not have any holes. Despite these results, the cathode basket was required to prevent dropped deposits from disturbing electrodes and other components in the electrorefiner, such as in test 1. In the case of tests 2 and 3, which employed the cathode basket, it was shown that only chloride salt and detached deposits were clearly observed inside the basket. Therefore, it is important to investigate methods to enhance the mass transfer rate when a cathode basket is installed to the electrorefiner. For example, a cathode basket can be manufactured to have a perforated structure, and electrolyte mixing systems can be applied to the electrorefiner.

Assuming that the weight ratio of Nb-94 to Nb did not change due to its long half-life, the radioactivity concentration of Nb-94 was proportional to the weight concentration in the irradiated CANDU pressure tube and the cathode deposit. Based on the ORIGEN-2 code calculation, the weight concentration of Nb and the radioactivity concentration of Nb-94 in the irradiated CANDU pressure tube after 10 years of cooling were shown as 2.364 wt. % and 8.345×10^6 Bq/g. Therefore, the radioactivity concentrations of Nb-94 in the cathode deposit obtained by electrorefining tests 2 and 3 were estimated as 85 and 448 Bq/g. These low concentrations could be attributed to the low amount of recovered Zr. Meanwhile, the radioactivity concentrations of Nb-94 could not be determined due to the very low Nb content in the deposit from test 1, which had a much higher recovery yield than tests 2 and 3. Further investigations with a cathode basket are required to increase the cathode yield.

6. Conclusions

For volumetric decontamination of the CANDU pressure tube, Zr separation was performed from Zr-2.5Nb alloy by anode potentiostatic electrorefining. Prior to electrorefining, the radioactive characteristics of the irradiated CANDU pressure tube were analyzed by utilizing the ORIGEN-2 code, and Nb was determined for consideration in electrorefining. Three potentiostatic electrorefining tests were designed with a variation in the surface area ratio of the cathode to the anode. The applied potential was set as −0.9 V (vs. Ag/AgCl 1 wt. %) at the anode. The cathode basket was installed for tests 2 and 3 to collect detached cathode deposits. The electrorefining results indicate that Zr could be recovered with limited concentrations of Nb and minor alloying elements in the early stages of electrorefining, as per expectations. The cathode forms were identified as Zr metal or a mixture of Zr and ZrCl, depending on the experimental conditions related to the overpotential. The deposits, which easily detached from the cathode and settled to the bottom, could be well collected by the installed cathode basket.

Author Contributions: Conceptualization, J.H., S.J. and I.S.H.; methodology, J.H. and S.J.; validation, J.H., S.J. and S.S.; formal analysis, J.H. and S.J.; investigation, J.H. and S.J.; resources, I.S.H.; data curation, J.H. and S.S.; writing—original draft preparation, J.H., S.J. and S.S.; writing—review and editing, S.S. and J.P.; visualization, J.H.; supervision, S.S. and I.S.H.; project administration, I.S.H.; funding acquisition, S.S. and I.S.H. All authors have read and agreed to the published version of the manuscript.

Funding: This work was supported by the National Research Foundation of Korea (NRF) grant funded by the Korean government (MSIP) (NRF-2017M2A8A5015147).

Institutional Review Board Statement: Not applicable.

Informed Consent Statement: Not applicable.

Data Availability Statement: Not applicable.

Conflicts of Interest: The authors declare no conflict of interest.

References

1. Nuclear Data Center at Korea Atomic Energy Research Institute. Table of Nuclides. Available online: http://atom.kaeri.re.kr:8080 (accessed on 2 March 2021).
2. Bradley, E.R.; Sabol, G.P. *Zirconium in the Nuclear Industry: Eleventh International Symposium*; ASTM: West Conshohocken, PA, USA, 1996.
3. NSSC Notice No. 2020-6. *Regulation on the Criteria for the Classification and Clearance of Radioactive Wastes*; Nuclear Safety and Security Commission: Seoul, Korea, 2020. (In Korean)
4. Jeon, M.K.; Lee, C.H.; Park, C.J.; Choi, J.H.; Cho, I.H.; Kang, K.H.; Park, H.-S.; Park, G.I. Effect of burn-up on the radioactivation behavior of cladding hull materials studied using the ORIGEN-S code. *J. Radioanal. Nucl. Chem.* **2013**, *298*, 1629–1633. [CrossRef]
5. Rudisill, T.S. Decontamination of Zircaloy cladding hulls from spent nuclear fuel. *J. Nucl. Mater.* **2009**, *385*, 193–195. [CrossRef]
6. Kroll, W.J.; Schlechten, A.W.; Yerkes, L.A. Ductile zirconium from zircon sand. *Trans. Electrochem. Soc.* **1946**, *89*, 263. [CrossRef]
7. Kroll, W.J.; Schlechten, A.W.; Carmody, W.R.; Yerkes, L.A.; Holmes, H.P.; Gilbert, H.L. Recent progress in the metallurgy of malleable zirconium. *Trans. Electrochem. Soc.* **1947**, *92*, 99. [CrossRef]
8. Jeon, M.; Kang, K.; Park, G.; Lee, Y. Chlorination reaction behavior of Zircaloy-4 hulls: Experimental and theoretical approaches. *J. Radioanal. Nucl. Chem.* **2012**, *292*, 513–517. [CrossRef]
9. Borjas Nevarez, R.; McNamara, B.; Poineau, F. Recovery of Zirconium from Zircaloys Using a Hydrochlorination Process. *Nucl. Technol.* **2021**, *207*, 263–269. [CrossRef]
10. Poineau, F. *Purification of Zirconium Cladding Using a Chloride Volatility Process (No. 15-8111)*; University of Nevada: Las Vegas, NV, USA, 2019.
11. Fujita, R.; Nakamura, H.; Haruguchi, Y.; Takahashi, R.; Utsunomiya, K.; Sato, M.; Ito, Y.; Goto, T.; Terai, T.; Ogawa, S. Development of a zirconium recycle process from zircaloy waste of a boiling water reactor (BWR). *Trans. At. Energy Soc. Jpn.* **2007**, *6*, 343–357. [CrossRef]
12. Park, K.T.; Lee, T.H.; Jo, N.C.; Nersisyan, H.H.; Chun, B.S.; Lee, H.H.; Lee, J.H. Purification of nuclear grade Zr scrap as the high purity dense Zr deposits from Zirlo scrap by electrorefining in LiF–KF–ZrF_4 molten fluorides. *J. Nucl. Mater.* **2013**, *436*, 130–138. [CrossRef]
13. Lee, C.H.; Kang, D.Y.; Jeon, M.K.; Kang, K.H.; Paek, S.W.; Ahn, D.H.; Park, K.T. Addition effect of fluoride compounds for Zr electrorefining in LiCl–KCl molten salts. *Int. J. Electrochem. Sci.* **2016**, *11*, 566–576.
14. Sakamura, Y. Zirconium behavior in molten LiCl-KCl eutectic. *J. Electrochem. Soc.* **2004**, *151*, C187. [CrossRef]
15. Park, J.; Choi, S.; Sohn, S.; Kim, K.R.; Hwang, I.S. Cyclic voltammetry on zirconium redox reactions in LiCl-KCl-$ZrCl_4$ at 500° C for electrorefining contaminated zircaloy-4 cladding. *J. Electrochem. Soc.* **2013**, *161*, H97. [CrossRef]
16. Park, J.; Choi, S.; Sohn, S.; Hwang, I.S. Cyclic voltammetry on Zr, Sn, Fe, Cr and Co in LiCl-KCl salts at 500° C for electrorefining of irradiated zircaloy-4 cladding. *J. Electrochem. Soc.* **2017**, *164*, D744. [CrossRef]
17. Han, W.; Wang, W.; Li, M.; Wang, J.; Sun, Y.; Yang, X.; Zhang, M. Electrochemical behavior and extraction of zirconium on Sn-coated W electrode in LiCl-KCl melts. *Sep. Purif. Technol.* **2020**, *232*, 115965. [CrossRef]

18. Lee, C.H.; Kang, K.H.; Jeon, M.K.; Heo, C.M.; Lee, Y.L. Electrorefining of zirconium from zircaloy-4 cladding hulls in LiCl-KCl molten salts. *J. Electrochem. Soc.* **2012**, *159*, D463. [CrossRef]
19. Sohn, S.; Park, J.; Hwang, I.S. Electrolytic recovery of high purity Zr from radioactively contaminated Zr alloys in chloride salts. *Int. J. Electrochem. Sci.* **2018**, *13*, 3897–3909. [CrossRef]
20. Sohn, S.; Choi, S.; Park, J.; Hwang, I.S. Computational model-based design of molten salt electrorefining process for high-purity zirconium metal recovery from spent nuclear fuel. *Int. J. Energy Res.* **2020**, 1–16. [CrossRef]
21. Croff, A.G. *User's Manual for the ORIGEN2 Computer Code (No. ORNL/TM—7175)*; Oak Ridge National Lab.: Oak Ridge, TN, USA, 1980.
22. IAEA-TECDOC-1037. *Assessment and Management of Ageing of Major Nuclear Power Plant Components Important to Safety: CANDU Pressure Tubes*; IAEA: Vienna, Austria, 1998.
23. ASTM B353-12. *Standard Specification for Wrought Zirconium and Zirconium Alloy Seamless and Welded Tubes for Nuclear Service (Except Nuclear Fuel Cladding)*; ASTM: West Conshohocken, PA, USA, 2017. [CrossRef]
24. Lantelme, F.; Barhoun, A.; Chevalet, J. Electrochemical behavior of solutions of niobium chlorides in fused alkali chlorides. *J. Electrochem. Soc.* **1993**, *140*, 324. [CrossRef]
25. Mohamedi, M.; Sato, Y.; Yamamura, T. Examination of niobium electrochemistry from the reduction of Nb_3Cl_8 in molten LiCl–KCl eutectic. *Electrochim. Acta* **1999**, *44*, 1559–1565. [CrossRef]
26. Jeong, G.Y.; Sohn, S.; Jeon, Y.; Park, J. Understanding of electrochemical behaviors of niobium in molten LiCl–KCl eutectic for pyrochemical decontamination process. *J. Nucl. Mater.* **2019**, *524*, 39–53. [CrossRef]
27. Cha, H.L.; Yun, J.I. Redox behaviors of zirconium in molten LiCl-KCl eutectic salt based on the comproportionation reaction between Zr (0) and Zr (IV). *Electrochem. Commun.* **2017**, *84*, 86–89. [CrossRef]